Supplementary Information

For

Interplay between Intrinsic Thermal Stability and Expansion Properties of Functionalized UiO-67 Metal-Organic Frameworks

Isabella Goodenough,[†] Venkata Swaroopa Datta Devulapalli,[†] Wenqian Xu[§*], Mikaela C. Boyanich,[†] Tian-Yi Luo,[‡] Mattheus De Souza,[‡] Mélissandre Richard,[†] Nathaniel L. Rosi,[‡] and Eric Borguet[†*]

[†]Department of Chemistry, Temple University, Philadelphia, Pennsylvania 19122, USA
[‡]Department of Chemistry, University of Pittsburgh, Pittsburgh, Pennsylvania 15260, USA
[§]X-ray Science Division, Advanced Photon Source, Argonne National Laboratory, Lemont, Illinois, 60439, USA

Sections in this Document

1. Fourier Transform Infrared Spectroscopy (FTIR)

1.1 UiO-67 Vibrational Modes

Table S1: Assignment of Infrared Vibrational Modes (cm^{-1}) of UiO-67 Series MOFs

Vibrational Mode [a]	UiO-67	UiO-67-NH_2	UiO-67-CH_3
$\nu(O\text{-}H)_{free}$	3678	3678	3678
$\nu_{as}(N\text{-}H)$	--	3485	--
$\nu_{s}(N\text{-}H)$	--	3398	--
$\nu(C\text{-}H)_{ring}$	3076	3074	3074
	3049	3051	3054
	3018	3016	3025
	2922	2925	2927
$\nu_{as}(C\text{-}H)_{me}$	--	--	2982
$\nu_{s}(C\text{-}H)_{me}$	--	--	2962
$\nu_{as}(OC\text{-}O)_{a.p}$	1670	1683	1683
$\beta(N\text{-}H)$	--	1627	--
$\nu_{s}(OC\text{-}O)_{i.p}$	1618	1615	1617
$\nu_{as}(C\text{-}O)$	1580	1577	1580
$\nu(C\text{-}C)_{ring}$	1535	1539	1533
$\nu_{s}(C\text{-}O)$	1360	1361	1356
$\nu(C\text{-}N)$	--	1270	--
$[\Upsilon(O\text{-}H) + \beta(C\text{-}H)]_{a.p}$	821	833	825
$[\beta(O\text{-}H) + \beta(C\text{-}H)]_{i.p}$	775	775	776
$\beta(O\text{-}H) + \nu(C\text{-}C)_{ring} + \beta(OC\text{-}O)$	715	719	714
$\nu(Zr\text{-}\mu_3\text{-}O)$	677	681	675
$\nu_{as}(Zr\text{-}OC)$	621	623	621
$\nu_{s}(Zr\text{-}OC)$	557	559	561
$\nu_{as}(Zr\text{-}\mu_3\text{-}OH)$	458	457	459
$\nu_{s}(Zr\text{-}\mu_3\text{-}OH)$	406	404	403

[a] IR band assignments are guided from [1-4]

ν = stretch, Υ = wagging, β = in-plane bending, as = asymmetric, s = symmetric, i.p = in-phase, a.p = anti-phase

1.2 Degassing and Sample Activation

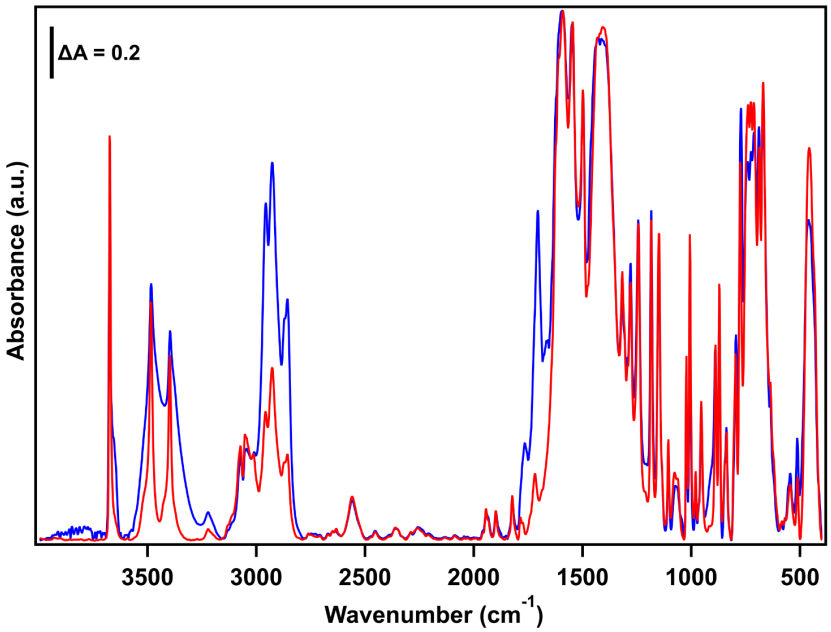

Figure S1 Full IR spectra of UiO-67-NH_2 recorded upon introduction to the UHV chamber ($P < 1.0 \cdot 10^{-6}$ Torr) (blue) and following sample activation at 473 K ($P < 1.0 \cdot 10^{-8}$ Torr) (red). All baseline corrected spectra were recorded at room temperature.

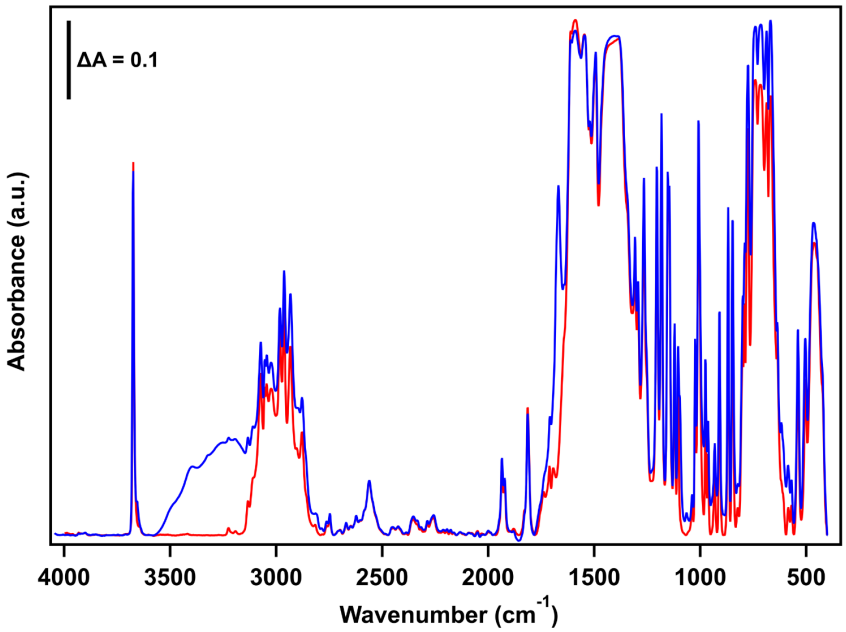

Figure S2 Full IR spectra of UiO-67-CH_3 recorded upon introduction to the UHV chamber ($P < 1.0 \cdot 10^{-6}$ Torr) (blue) and following sample activation at 473 K ($P < 1.0 \cdot 10^{-8}$ Torr) (red). All baseline corrected spectra were recorded at room temperature.

1.3 Reversible Thermal Effects

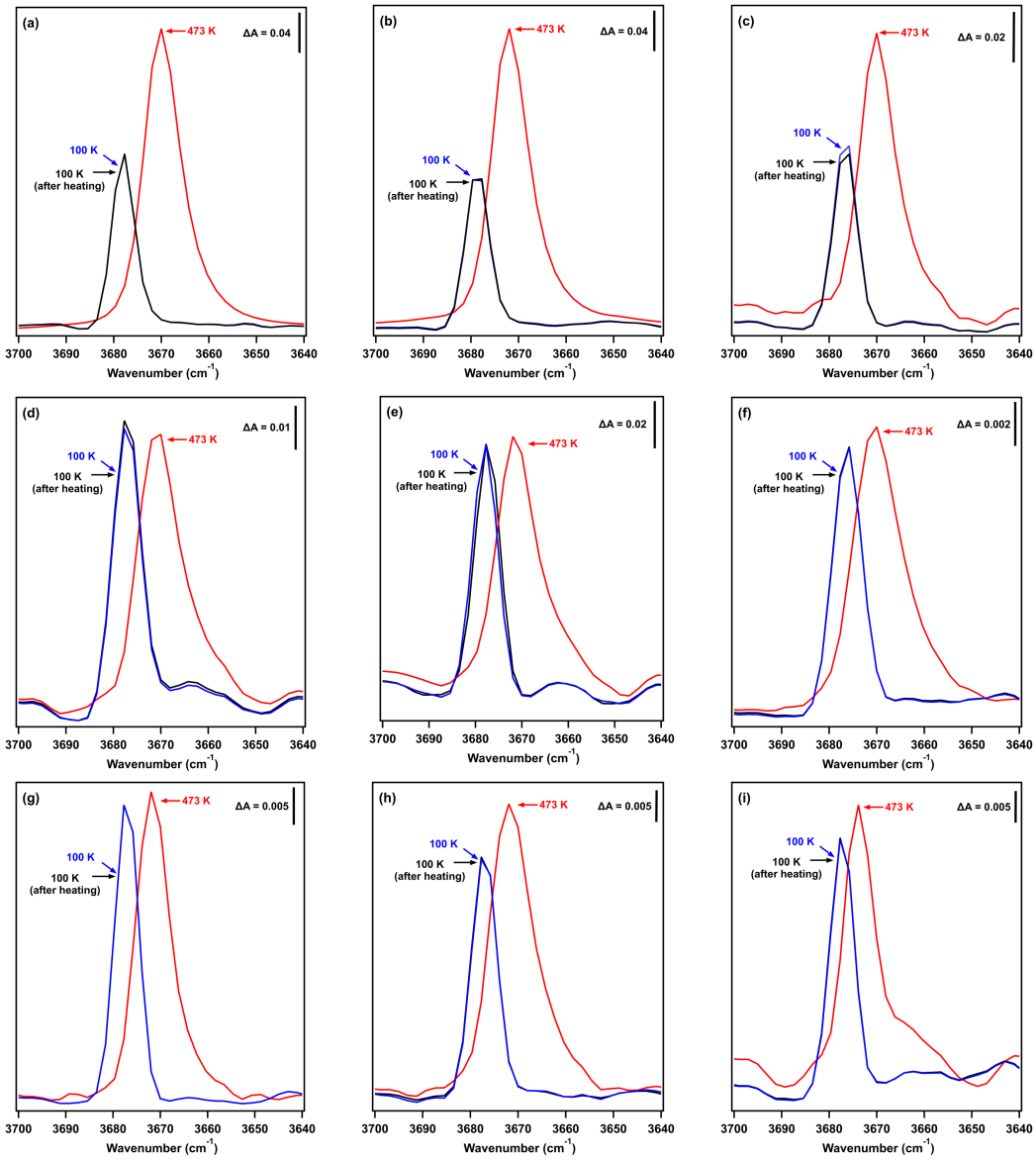

Figure S3 IR spectra recorded before heating at 100 K (blue), during heating at 473 K (red), and after cooling to 100 K (black) for UiO-67 (a-c), UiO-67-NH_2 (d-f) and UiO-67-CH_3 (g-i). Spectra were acquired on multiple dates from different sample batches to demonstrate reproducibility and reversibility of the intrinsic thermal behavior of the isolated μ_3-OH stretch, ($\nu(OH)_{free}$) at 3678 cm^{-1} (100 K)

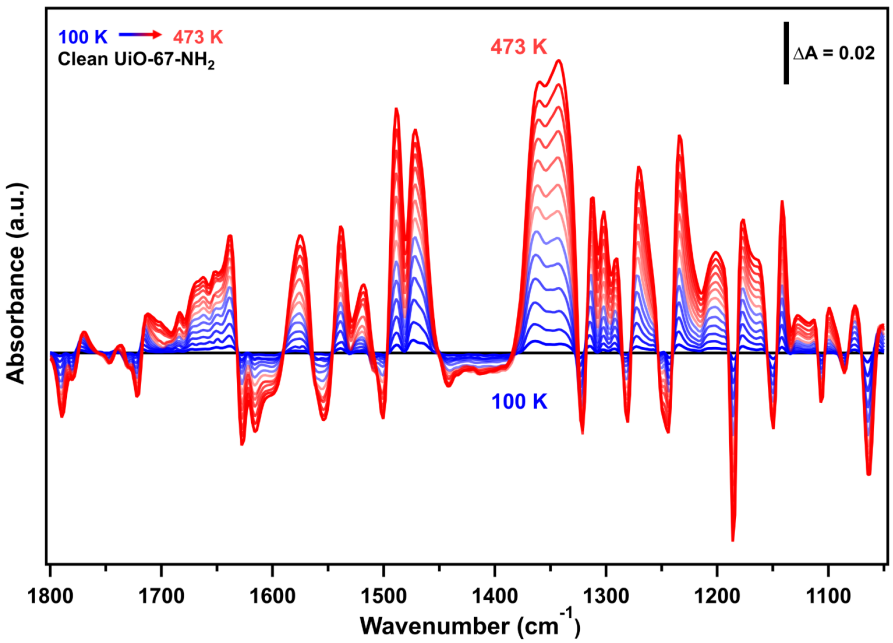

Figure S4 IR difference spectra for UiO-67-NH_2 in the 1800 – 1050 cm^{-1} region taken during heating from 100 K (blue) to 473 K (red) as indicated by the color legend showing changes in carboxylate and benzene ring stretching modes, C-H and N-H bending modes. Spectra were collected using the clean MOF at 100 K as the reference.

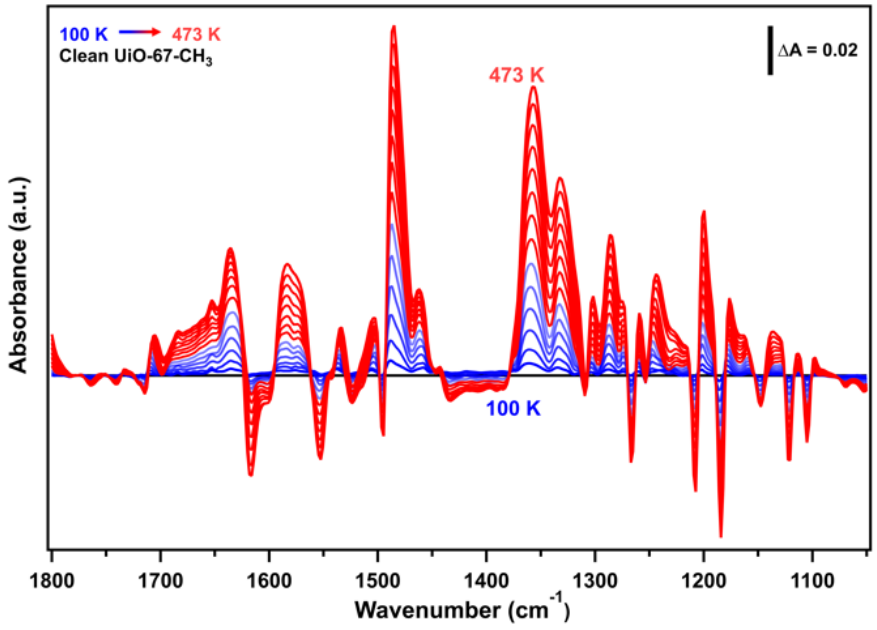

Figure S5 IR difference spectra for UiO-67-CH_3 in the 1800 – 1050 cm^{-1} region taken during heating from 100 K (blue) to 473 K (red) as indicated by the color legend showing changes in carboxylate and benzene ring stretching modes, and C-H bending modes. Spectra were collected using the clean MOF at 100 K as the reference.

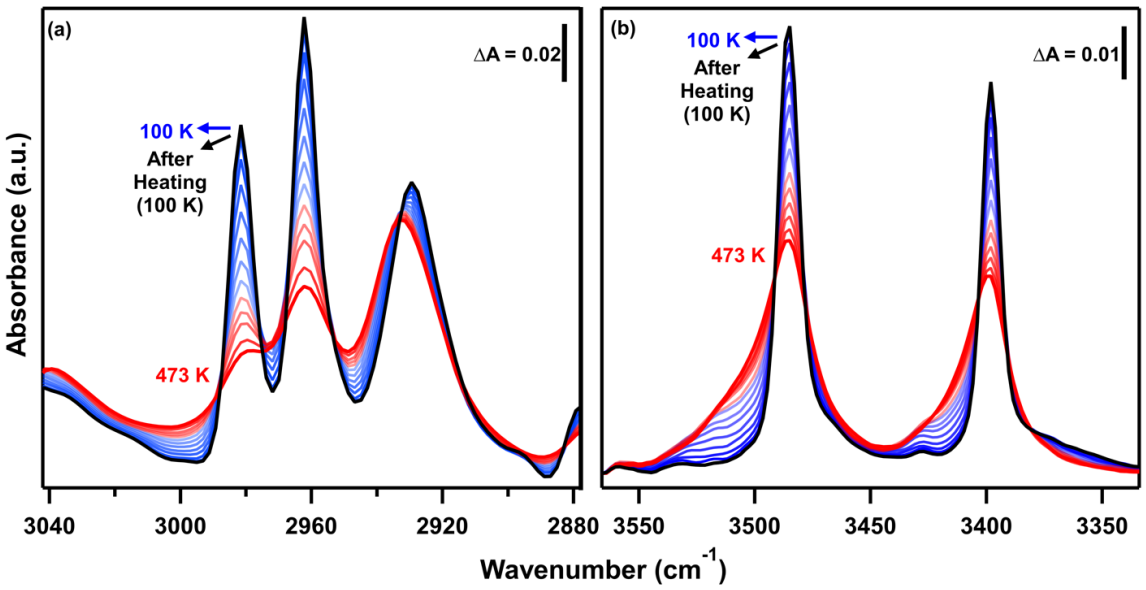

Figure S6 IR spectra recorded *in situ* during heating from 100 K (blue) to 473 K (red) and after sample heating (100 K) (black). (a) methyl C-H stretching between 3040 cm^{-1} – 2880 cm^{-1} of UiO-67-CH_3 for ν_{as}(C-H) and ν_s(C-H), respectively; (b) primary N-H stretching between 3550 cm^{-1} – 3350 cm^{-1} of UiO-67-NH_2 for ν_{as}(N-H) and ν_s(N-H), respectively. After cooling to 100 K, the initial breadth and intensity are recovered for all spectral features. All spectra are baseline corrected.

1.4 Irreversible Thermal Effects

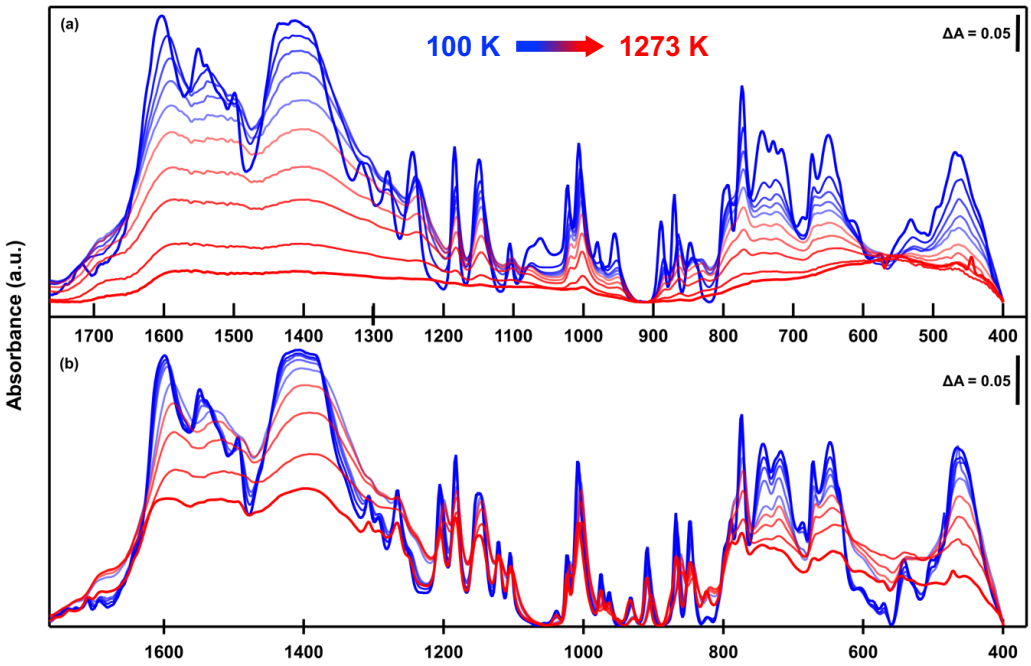

Figure S7 IR spectra recorded during heating from 300 K to 1273 K for (a) UiO-67-NH_2 and (b) UiO-67-CH_3 showing the temperature dependent spectral changes for MOF skeletal modes between 1750 cm^{-1} – 400 cm^{-1}. All baseline corrected spectra are presented for increasing temperature from blue to red as indicated by the color legend.

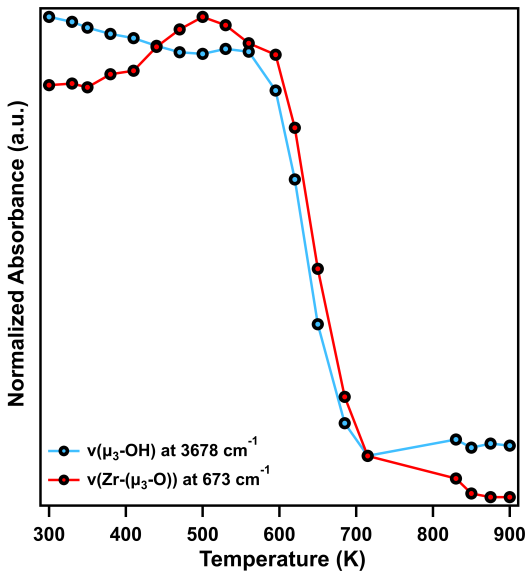

Figure S8 Normalized IR spectral intensity of the μ_3-OH stretch at 3678 cm^{-1} and Zr-(μ_3-O) stretch at 673 cm^{-1} for UiO-67 during heating from 300 K to the point of complete dehydroxylation (~900 K)

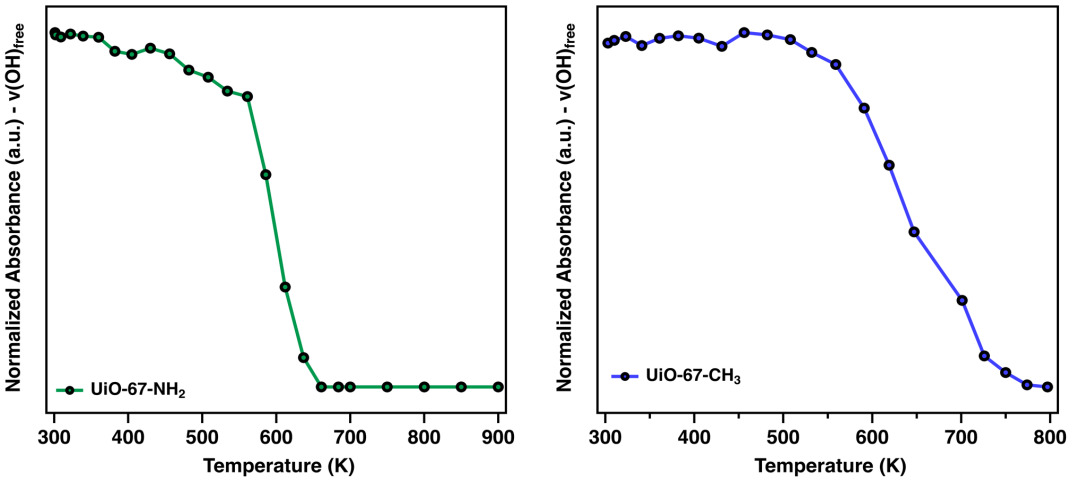

Figure S9 Normalized IR spectral intensity of the μ_3-OH stretch at 3678 cm^{-1} for UiO-67-NH_2 (green, left) and UiO-67-CH_3 (blue, right) as a function of temperature.

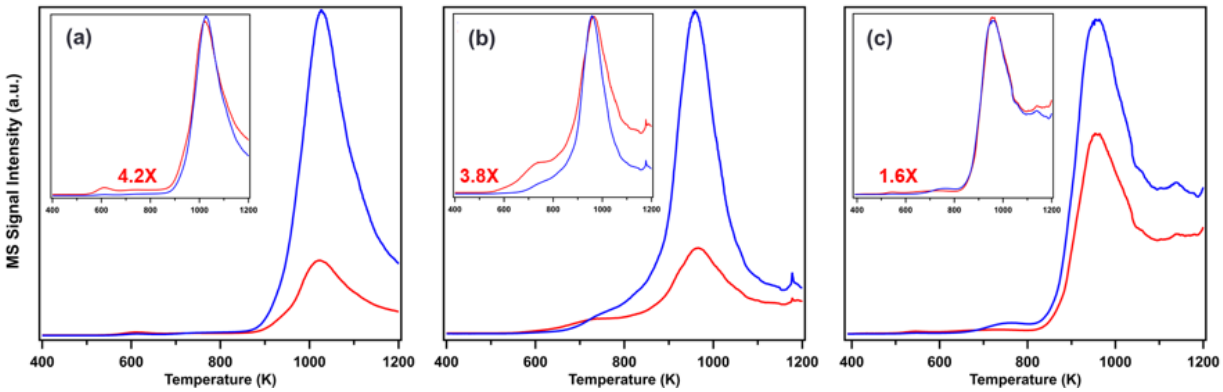

Figure S10 TPD-MS profiles for (a) UiO-67, (b) UiO-67-NH_2 and (c) UiO-67-CH_3 showing the CO_2^+ (m/z = 44, blue trace) and CO^+ (m/z = 28, red trace) molecular ion fragments during heating from 300 K – 1273 K.

2. In situ X-ray Diffraction

2.1. Synchrotron *in situ* XRD Data analysis

The TOPAS (version 5) software was used for Rietveld refinement and sequential refinement. The scattering profile of an empty capillary was subtracted from each data pattern to ease the fitting of the background line in the refinement process. The background was fitted using a 14-term Chebyshev polynomial. Peak profiles were fitted using the Pseudo-Voigt function. The initial structure models of UiO-67, UiO-67-NH_2 and UiO-67-CH_3 were constructed based a previously published structure of UiO-67.[5] The ligands were modeled as rigid bodies with limited flexibility on bond lengths and angles in the ligand and the torsion angle between the carboxylate and the benzene ring. Zr and μ_3-O (H) were refined as independent atoms. Hydrogen atoms were included in the structure models but attached to the associated C or O with fixed bond lengths and angles. Hydrogen atoms are usually excluded in powder XRD data analysis due to data resolution. However, the fit of the UiO-67 data in this study is improved when the hydrogen atoms are included. Three to four independent variables were used to model the atomic displacement parameters (ADPs) of all the atoms in the structures, one for Zr, one for all the atoms in the ligand except the oxygen atoms, and one or two for the oxygen atoms. When two variables were used for O, one is for μ_3-O (H) and the other is for the terminal O.

2.2 Temperature cycling experiment

The activation at 473 K (373 K for UiO-67-CH_3) removed almost all the absorbed solvent molecules in the frameworks, but was also gradually decreasing sample crystallinity as the samples were kept at the activation temperature. To preserve the crystallinity and in order to retrieve the greatest amount of structural information from the XRD data, the samples were cooled from the activation temperature to 300 K as soon as the low 2θ angle XRD peaks showed no more changes in intensity (~10 min), indicating the absorbed molecules in the frameworks were mostly removed. **Figure S11** shows the response of low angle peaks of UiO-67 during the activation process. Refinement with the activated UiO-67 data shows μ_3-O of the Zr_6 cluster can be better fitted with two oxygen sites (O1a and O1b) to differentiate the oxygen atom and the hydroxyl group. It also reveals the presence of diffuse electron density in the tetrahedral pores of the framework close to

the μ_3-O, indicating a small amount of highly disordered absorbed species not removed by the activation. The absorbed species is represented by an isolated oxygen atom (Ow1) with a fixed site occupancy of 0.52, a number obtained from the refinement with the pattern at 90 K (**Figure S11 and S12**). The position and ADP of Ow1 are refined in the sequential refinement. The site occupancies of all the C and H atoms in the BPDC linker are set to one parameter (referred to as the linker occupancy) in the refinement to indicate the possible scenario of missing linkers of the as-synthesized material or losing linkers in the heating process. No significant variation of the linker occupancy is observed in the sequential refinement. As a result, the linker occupancy parameter is fixed to 0.97, a value obtained from the refinement using the data at 90 K. The refinement with the UiO-67-NH_2 data follows the same strategy used for UiO-67. Electron density from solvent is also resolved in the tetrahedral pore of the activated UiO-67-NH_2 and modeled by the Ow1 site. The linker occupancy does not display significant variation in the preliminary refinement, and is set to 0.93, the refined value from the data taken at 90 K. The UiO-67-CH_3 data do not have as good resolution as the other two to refine the atomic positions to high accuracy, and only the refined unit cell parameters are reported.

2.3 Thermal degradation experiment

The samples in the degradation experiment are not pre-activated. A decent fit of the XRD profile of the initial UiO-67 is achieved by employing three oxygen sites, Ow1, Ow2, and Ow3, to simulate the electron density of the solvent molecules. The three sites are all in the tetrahedral pore. The octahedral pore, which is the bigger one of the two types of pores in the UiO-67 structure, appears to be empty of solvent. The occupancies of the three solvent oxygen sites decrease in the refinement with higher temperature data, and become nearly zero at 480 K. The solvent oxygen sites are removed from the refinement with the data above 480 K. To model the $Zr_6O_4(OH)_4$ dehydroxylation, μ_3-O (H) is modeled as one oxygen site (O1) with the site occupancy refined. At 480 K, the O1 site occupancy starts decreasing, and reaches a minimum of 0.78(2) at 580 K. The occupancy is fixed to 0.78 for the refinement with data at above 600 K. The evolution of linker occupancy was explored in the initial refinement and did not show significant variation until the final degradation at 810 K. The linker occupancy is fixed to 0.97 in the final refinement, the same value used in the temperature cycling experiment.

2.4 CIFs included in this submission

The following refined structures are reported as CIFs.

UiO67-2_90to480Ka_90K_d400-00000-sub0_9qtz: the structure of UiO-67 at 90 K from the temperature cycling experiment. The sample underwent a short activation at 473 K and cooled to 90 K.

UiO67-2_90to480Ka_480K_d400-00000-sub0_9qtz: the structure of UiO-67 at 480 K from the temperature cycling experiment. The sample underwent a short activation at 473 K and cooled to 90 K, then stepwise heated to 480 K.

UiO67NH2-4_90to480Ka_90K_d400-00000-sub0_9qtz: the structure of UiO-67-NH_2 at 90 K from the temperature cycling experiment. The sample underwent a short activation at 473 K and cooled to 90 K.

UiO67NH2-4_90to480Ka_480K_d400-00000-sub0_9qtz: the structure of UiO-67-NH_2 at 480 K from the temperature cycling experiment. The sample underwent a short activation at 473 K and cooled to 90 K, then stepwise heated to 480 K.

UiO67-4-00000-sub0_0360qtz: the structure of UiO-67 at room temperate from the thermal degradation experiment.

UiO67-4-00029-sub0_0360qtz: the structure of UiO-67 at 580 K from the thermal degradation experiment.

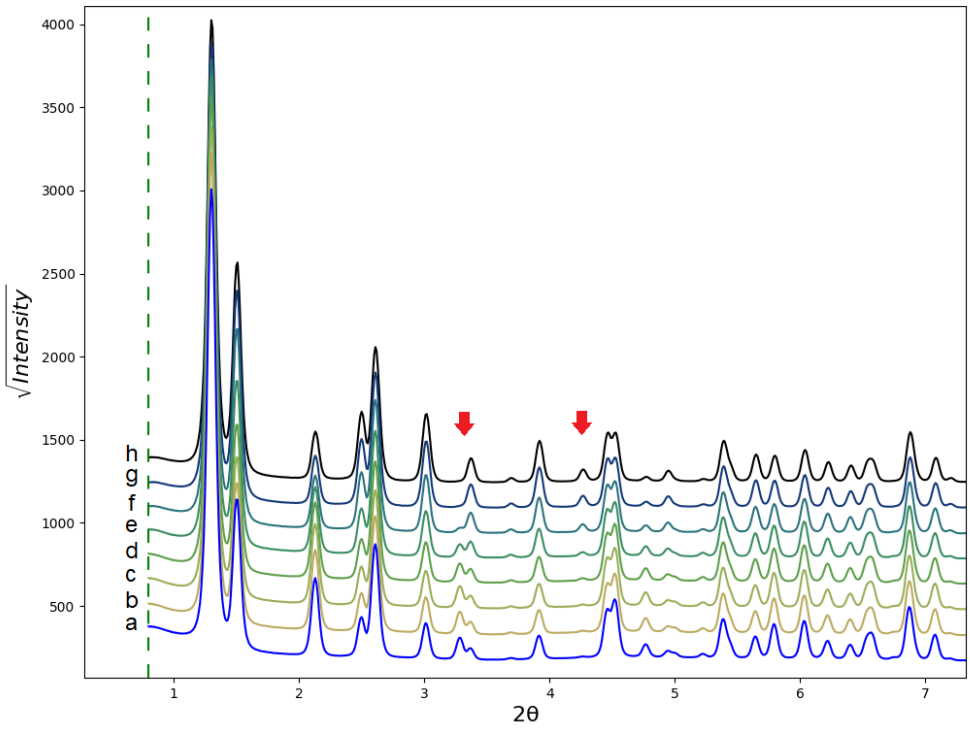

Figure S11 XRD patterns of UiO-67 during the activation process. Red arrows point to peaks reflecting the loss of physically absorbed species. (a) at ambient pressure at 300 K, under vacuum at (b) 300 K, (c) 314 K, (d) 372 K, (e) 413 K, (f) 447 K (g) 473 K and (h) after 2 minutes at 473 K.

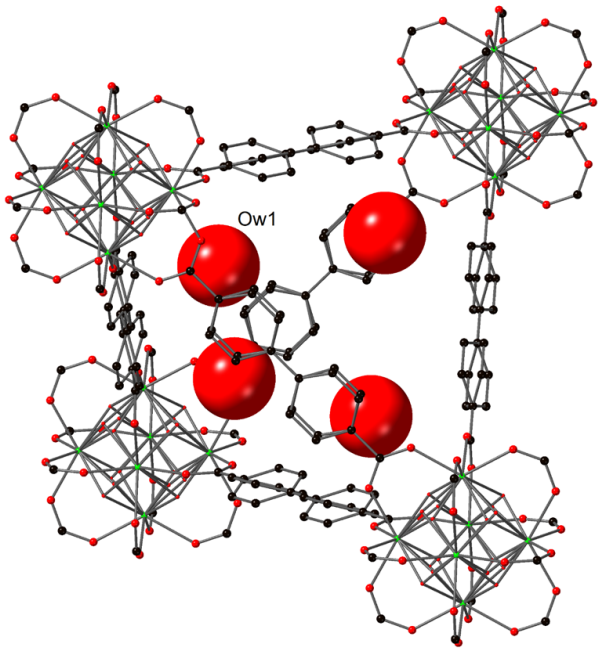

Figure S12 Structure of the activated UiO-67 measured at 90 K. The isolated oxygen atoms (Ow1) in the tetrahedral pore represent the remaining solvent molecules. The sphere size is proportional to the ADP.

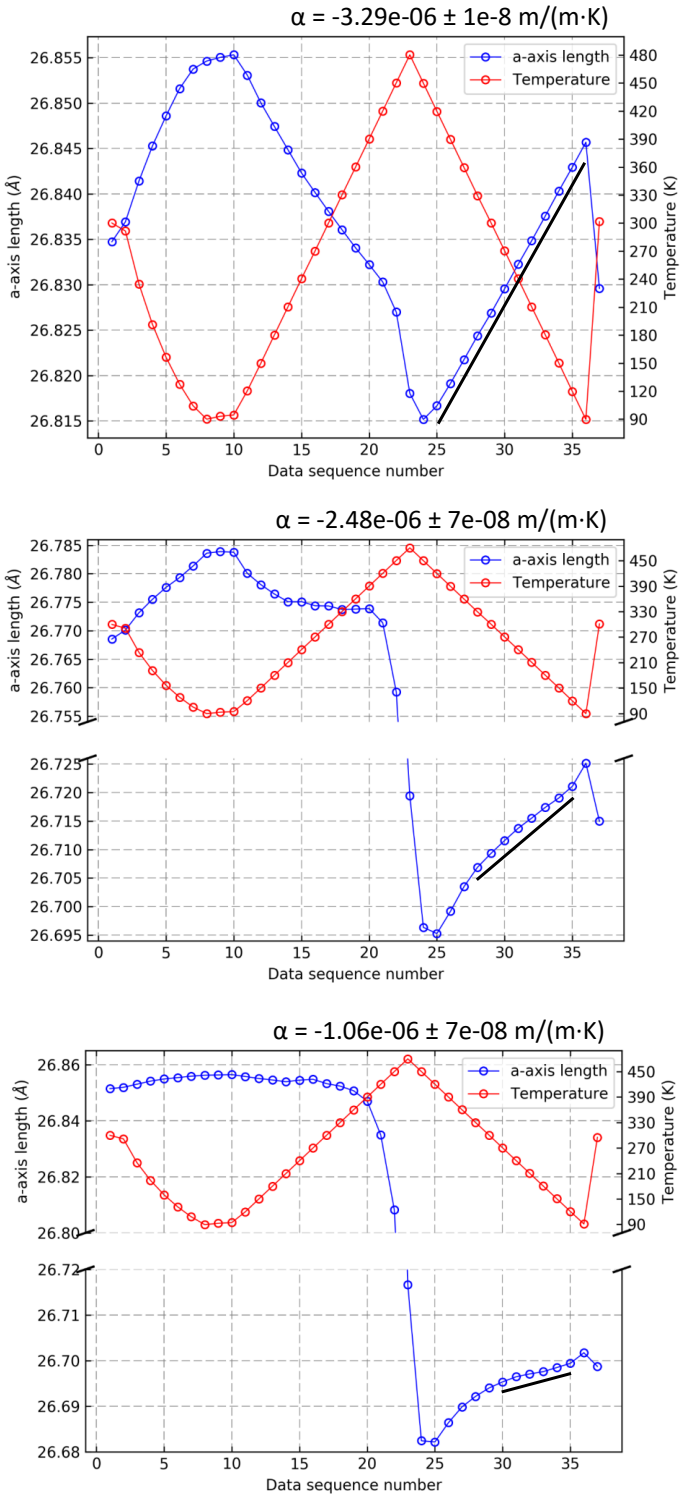

Figure S13 Evolution of unit cell edge length (Å) of UiO-67 (top), UiO-67-NH_2 (middle), and UiO-67-CH_3 (bottom) in the temperature cycling experiment. The linear thermal coefficient (α) was calculated for each MOF using data points marked by the black line. The associated error in the unit cell edge length (Å) is smaller than the symbol size.

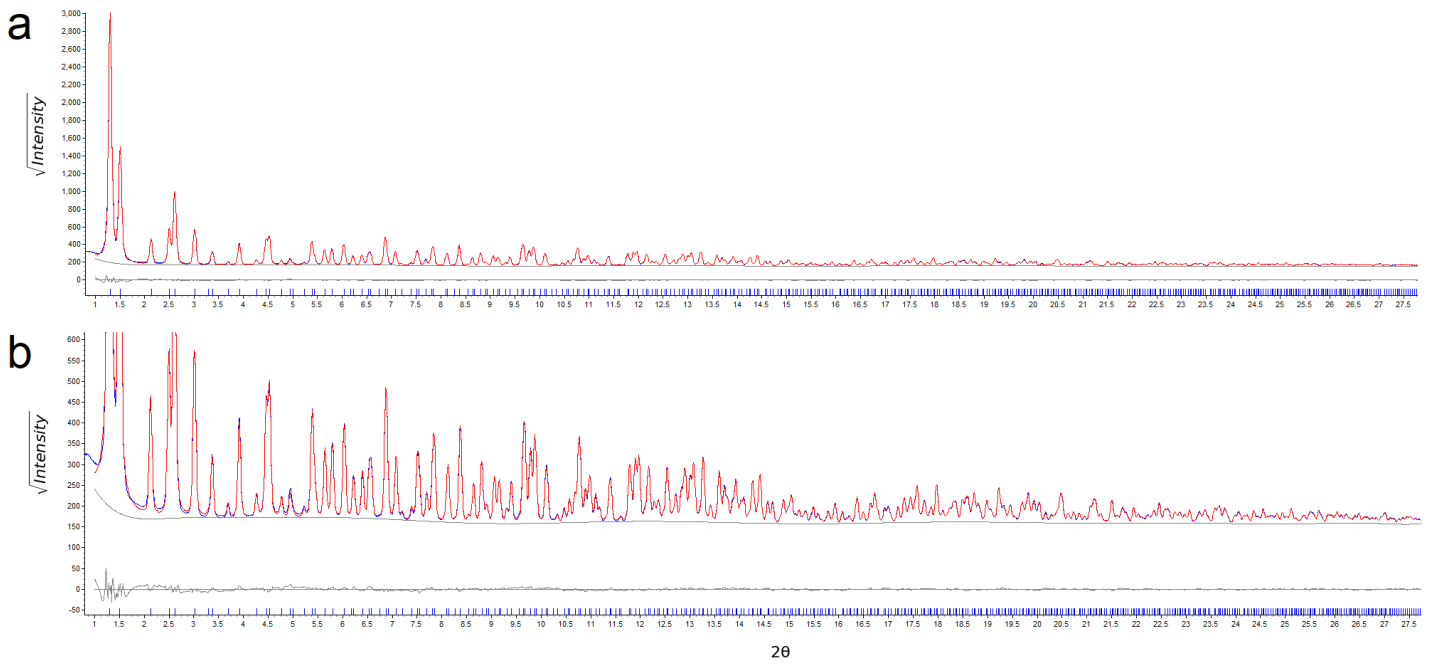

Figure S14 Refinement plots of activated UiO-67 at 90 K. (a) and (b) are the same refinement with (b) amplified to show the low intensity peaks. The data profile is in blue, and the calculated profile is in red. The grey line underneath the data profile is the refined background. The grey line at the bottom of each plot oscillating around zero is the difference curve.

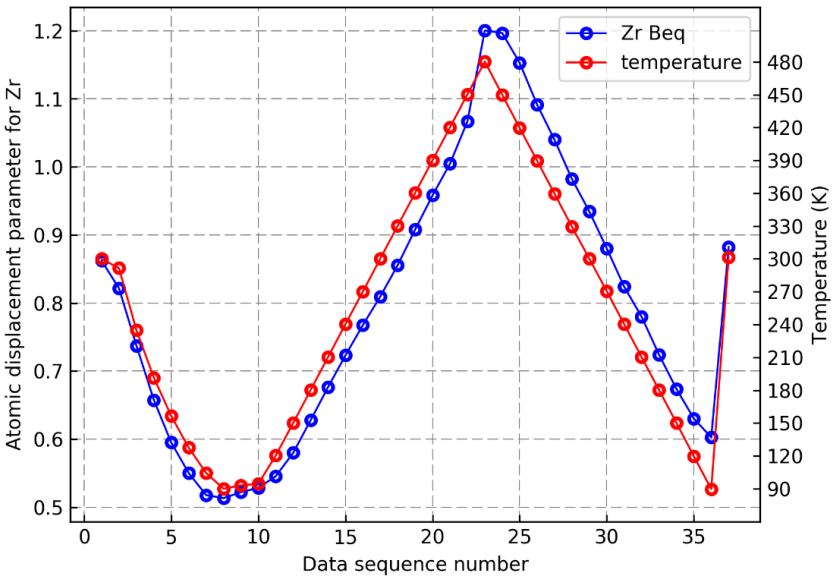

Figure S15 Evolution of the Zr ADP in the temperature cycling experiment. Note that the increase of the Zr ADP at ~480 K is associated with the non-linear decrease of the cell edge length shown in Figure S13. The irreversible increase signals an increase of static disorder of the Zr_6O_8 cluster. The associated error for the Zr ADP values is smaller than the symbol size.

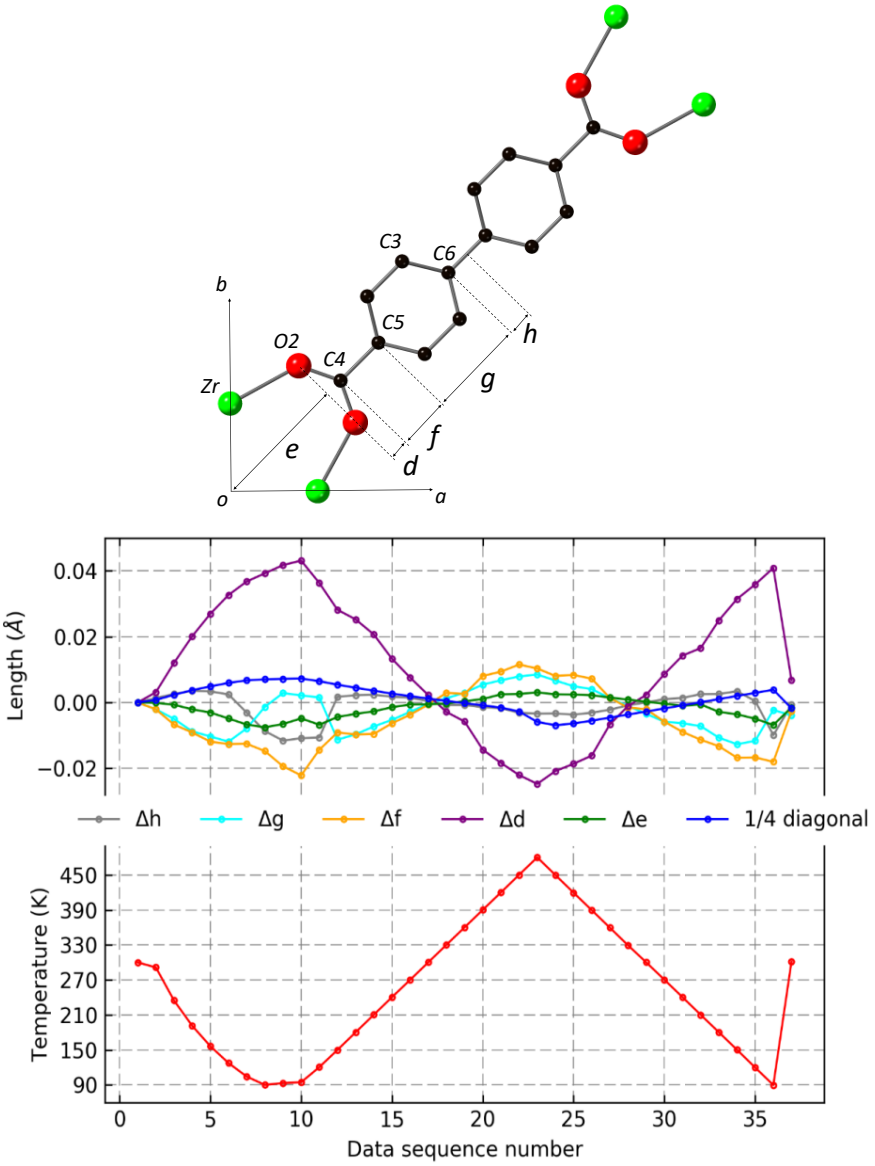

Figure S16 Part of the UiO-67 structure showing the connection of Zr node and the BPDC linker along the ab diagonal (Top) and evolution of the labeled distances in the temperature cycling experiment (Bottom). Note: h is the half of the C6-C6 bond length. The sum of d, e, f, g and h is equal to a quarter of the unit cell ab diagonal length. In the bottom plot, the change of d (Δd) is the only distance completely negatively correlated to the temperature profile and is the main contributor to the NTE of UiO-67. Error in the measured bond distances (Å) are smaller than the symbol size.

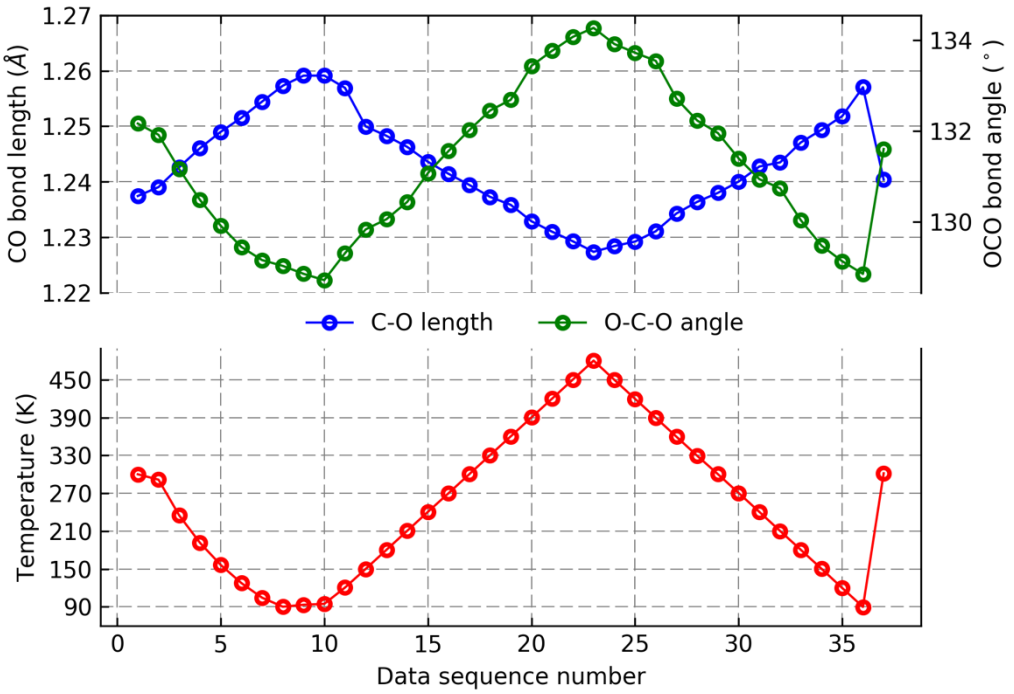

Figure S17 Evolution of the C-O bond length and the O-C-O bond angle of UiO-67 during the temperature cycling experiment. Error in the measured bond distances (Å) are smaller than the symbol size.

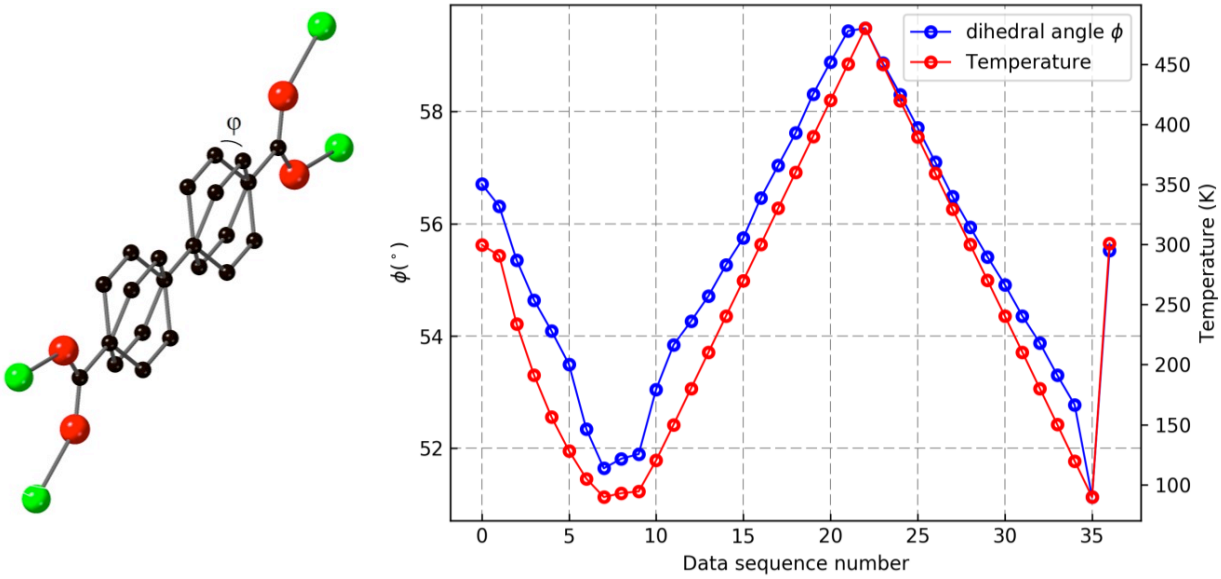

Figure S18 Evolution of the linker dihedral angle (φ) for UiO-67-NH_2 during the temperature cycling experiment. Error in the measured dihedral angle values (°) are smaller than the symbol size.

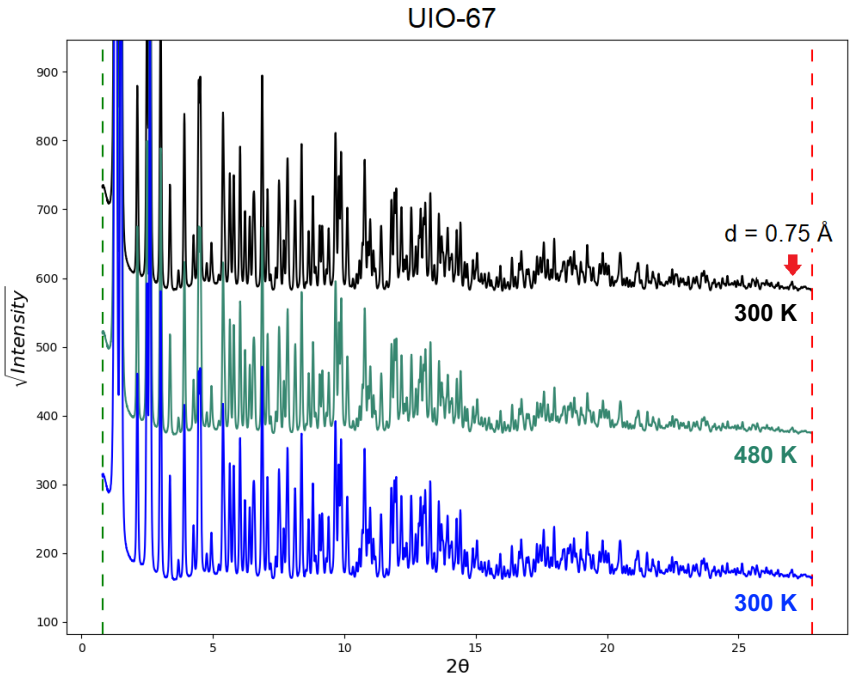

Figure S19 XRD profiles of UiO-67 during the temperature cycling experiment. Blue: the activated sample measured at 300 K. Cyan: at 480 K. Black: the sample measured after returning to 300 K. The temperature history is shown in Figure S13.

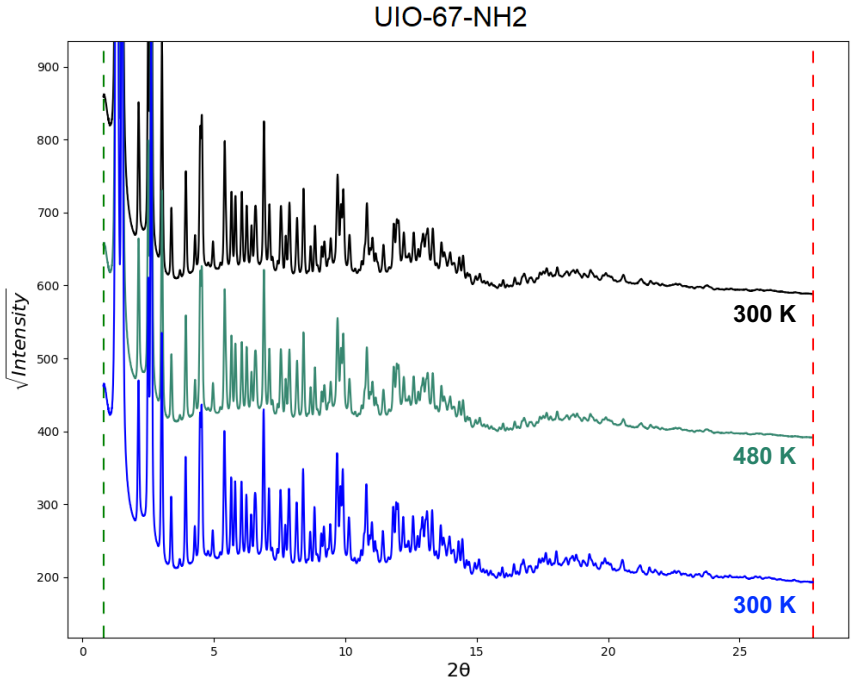

Figure S20 XRD profiles of UiO-67-NH_2 in the temperature cycling experiment. Blue: the activated sample measured at 300 K. Cyan: at 480 K. Black: the sample measured after returning to 300 K. The temperature history is in Figure S13.

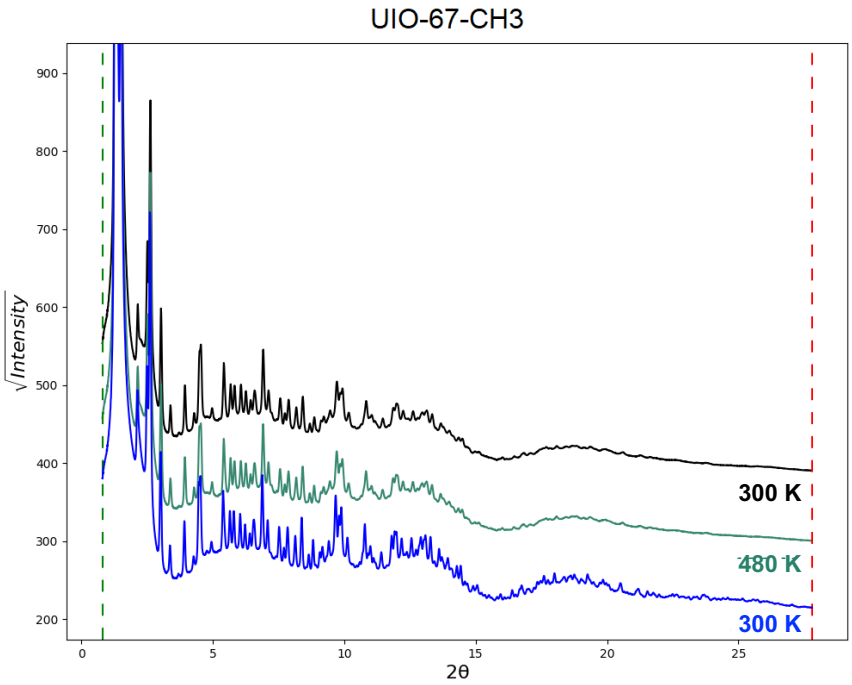

Figure S21 XRD profiles of UiO-67-CH_3 in the temperature cycling experiment. Blue: the activated sample measured at 300 K. Cyan: at 480 K. Black: the sample measured after returning to 300 K. The temperature history is in Figure S13.

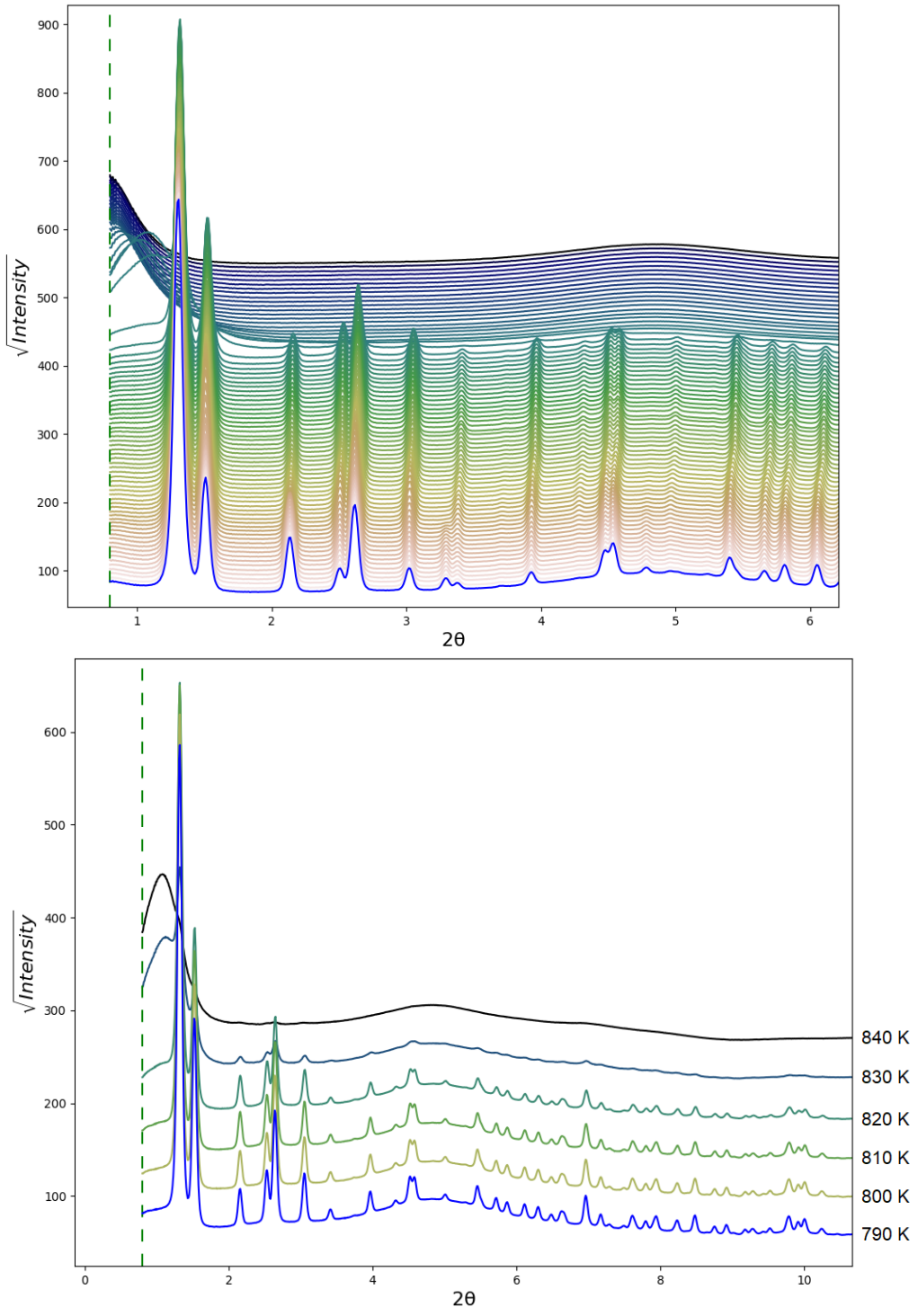

Figure S22 XRD profiles of UiO-67 in the thermal degradation experiment. The top panel shows the whole data series, and the bottom panels shows the patterns across the degradation point.

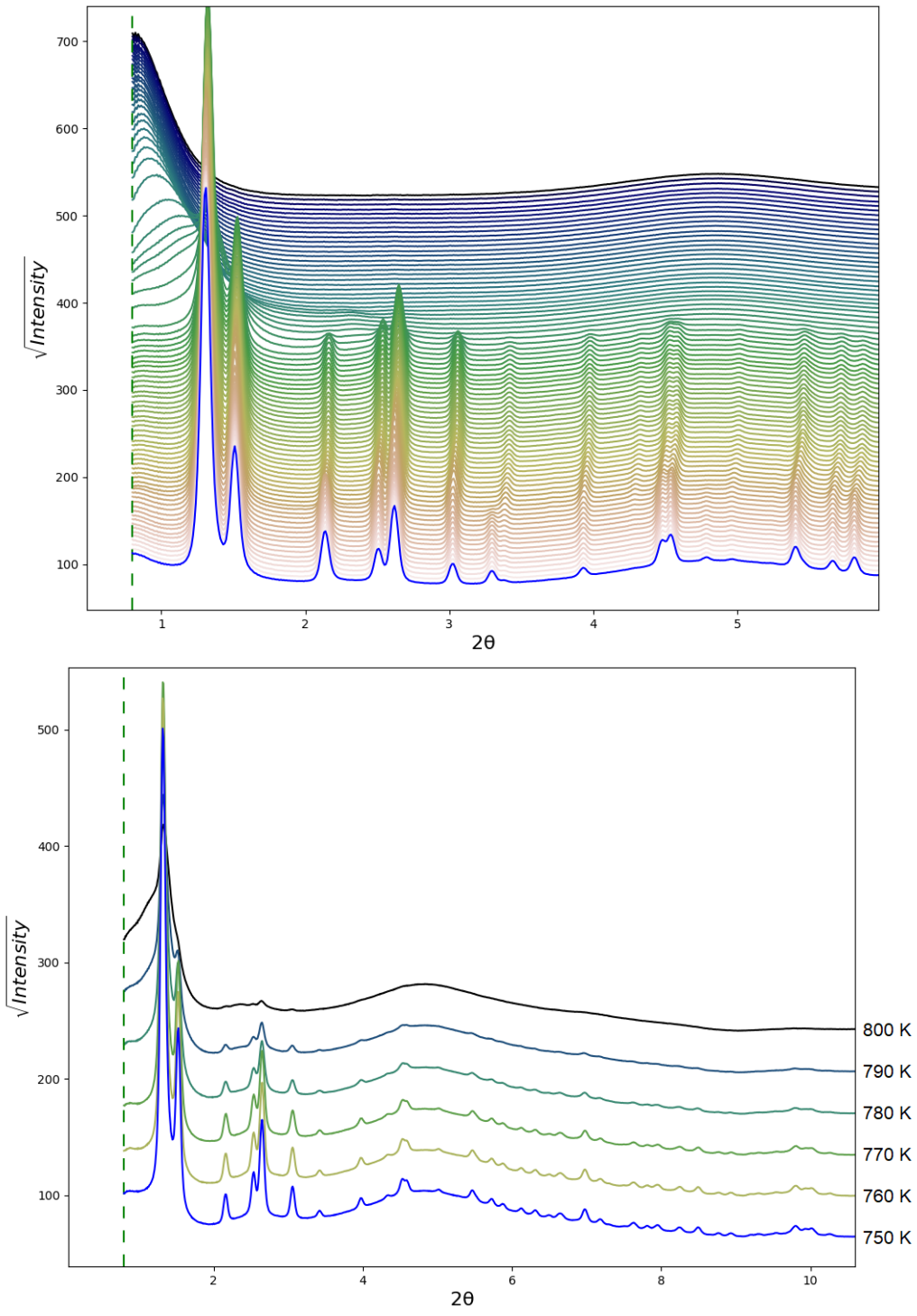

Figure S23 XRD profiles of UiO-67-NH_2 in the thermal degradation experiment. The top panel shows the whole data series, and the bottom panels shows the patterns across the degradation point.

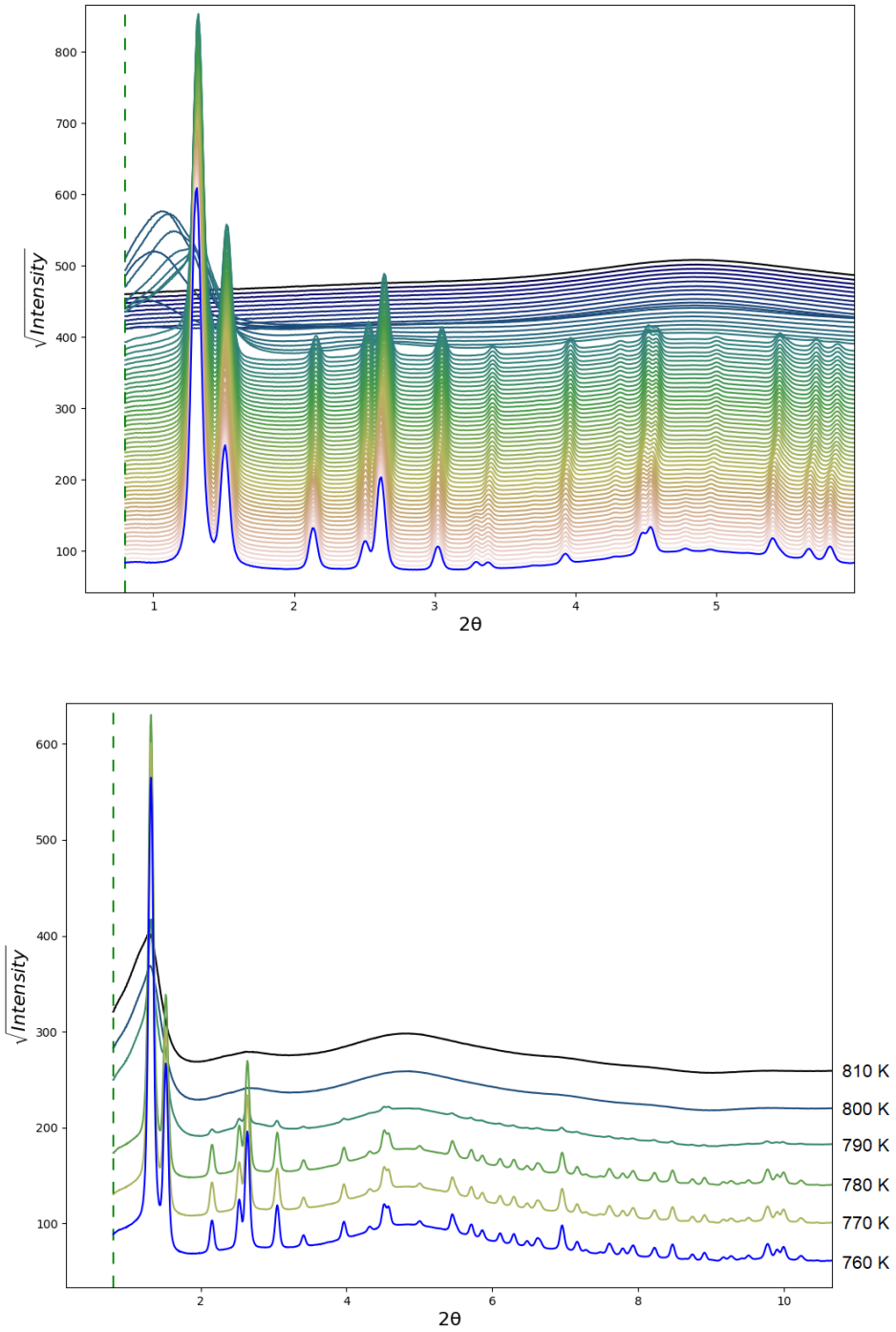

Figure S24: XRD profiles of UiO-67-CH_3 in the thermal degradation experiment. The top panel shows the whole data series, and the bottom panels shows the patterns across the degradation point.

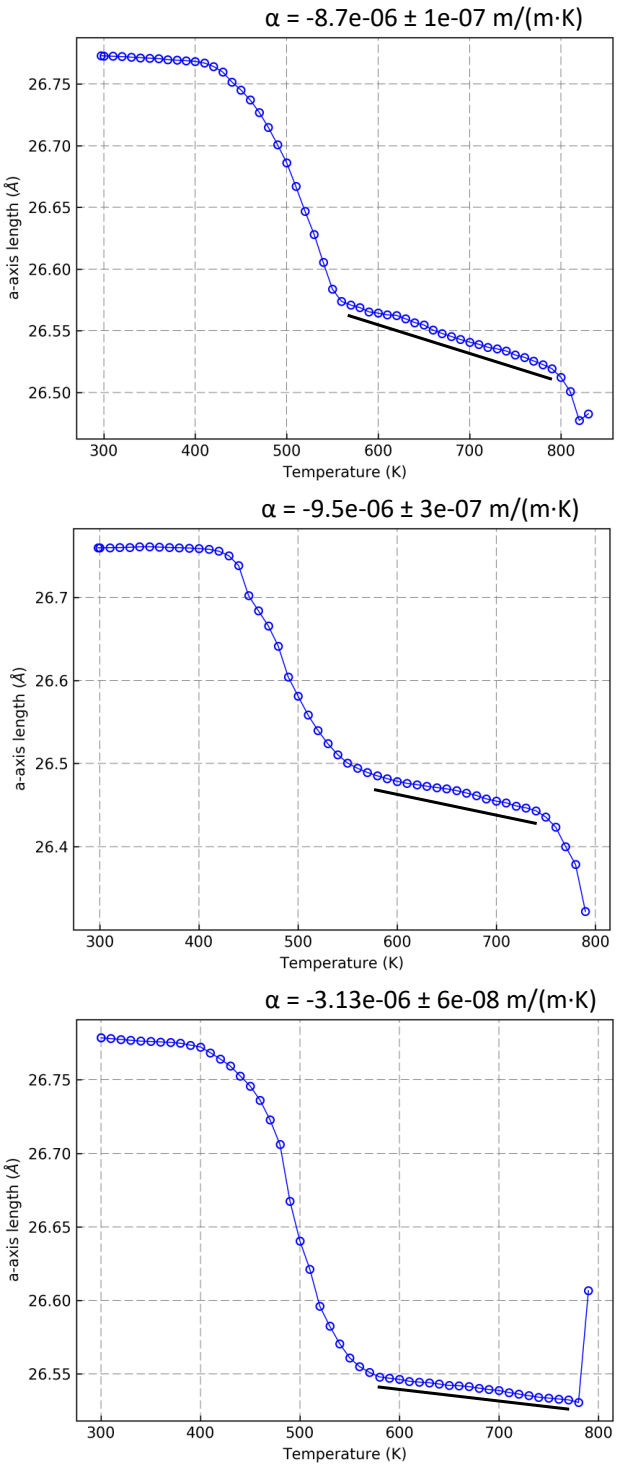

Figure S25: Evolution of unit cell edge length of UiO-67 (top), UiO-67-NH_2 (middle), and UiO-67-CH_3 (bottom) in the thermal degradation experiment. The associated error in the unit cell edge length (Å) is smaller than the symbol size. The linear thermal coefficient (α) was calculated for each MOF using data points marked by the black line

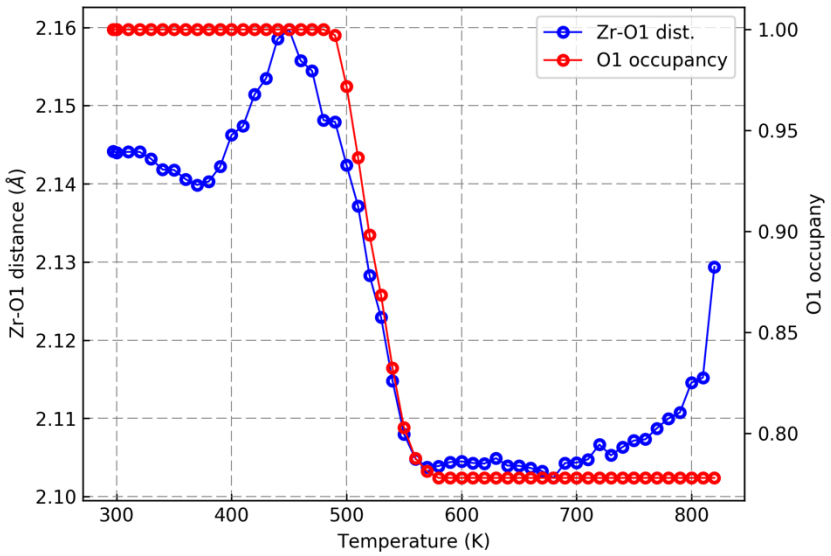

Figure S26: Change of the μ_3-O (H) site occupancy (O1 occupancy) and the average bond length between Zr and μ_3-O (H) as a function of temperature from the refinement results of the UiO-67 thermal degradation XRD data. The associated error in the measured bond length (Å) is smaller than the symbol size.

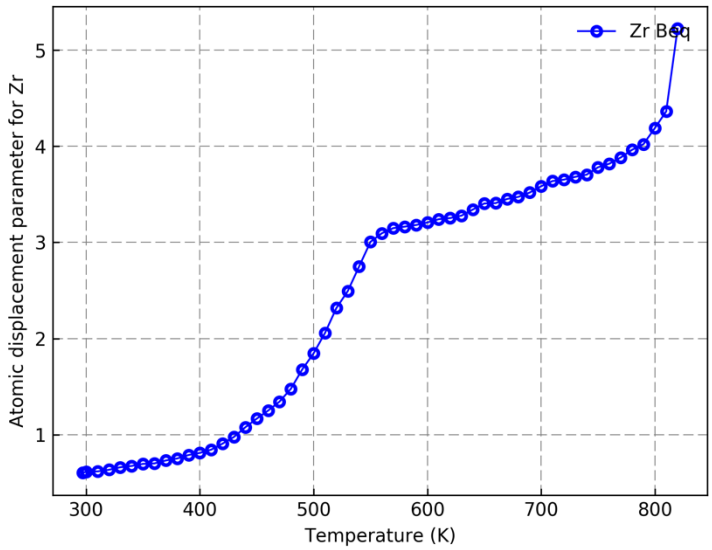

Figure S27: Evolution of the Zr ADP of UiO-67 in the thermal degradation experiment. Note the sharp increase of the Zr ADP from around 430 K to 550 K associated with the large contraction of cell edge length shown in Figure S25, indicating a drastic increase of the disorder on the Zr atomic site. The associated error for the Zr ADP values is smaller than the symbol size.

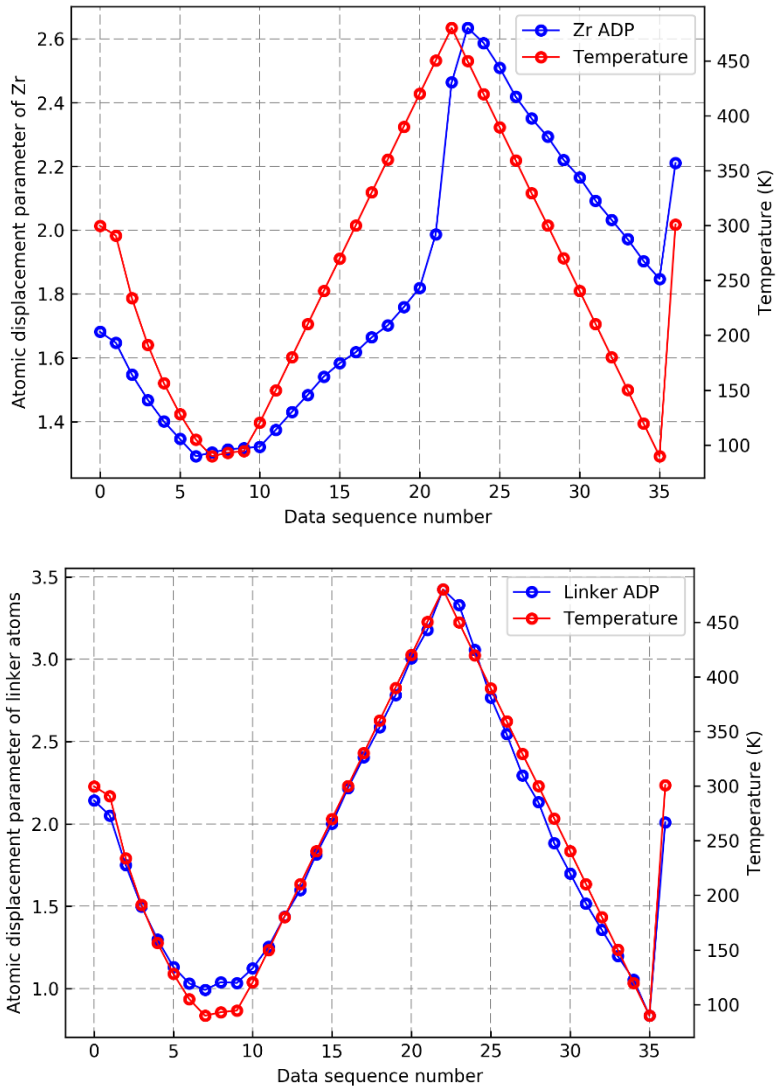

Figure S28: Variation of the atomic displacement parameters of UiO-67-NH_2 in the temperature cycling experiment. Note the Zr ADP has an irreversible increase at around 480 K, which is not seen in the linker ADP profile. The irreversible increase of Zr ADP is caused of the dehydroxylation of the Zr node that cause more disorders of the Zr atom. The Zr node dehydroxylation does not directly affect the linker, so the linker ADP is fully reversible with temperature. The associated error for the Zr and linker ADP values is smaller than the symbol size.

References:

1. Valenzano, L.; Civalleri, B.; Chavan, S.; Bordiga, S.; Nilsen, M. H.; Jakobsen, S.; Lillerud, K. P.; Lamberti, C., Disclosing the Complex Structure of UiO-66 Metal Organic Framework: A Synergic Combination of Experiment and Theory. *Chem. Mater.* **2011,** *23* (7), 1700-1718.
2. Shearer, G. C.; Forselv, S.; Chavan, S.; Bordiga, S.; Mathisen, K.; Bjorgen, M.; Svelle, S.; Lillerud, K. P., In Situ Infrared Spectroscopic and Gravimetric Characterisation of the Solvent Removal and Dehydroxylation of the Metal Organic Frameworks UiO-66 and UiO-67. *Top. Catal.* **2013,** *56* (9-10), 770-782.
3. Cavka, J. H.; Jakobsen, S.; Olsbye, U.; Guillou, N.; Lamberti, C.; Bordiga, S.; Lillerud, K. P., A New Zirconium Inorganic Building Brick Forming Metal Organic Frameworks with Exceptional Stability. *J. Am. Chem. Soc.* **2008,** *130* (42), 13850-13851.
4. Wang, G.; Sharp, C.; Plonka, A. M.; Wang, Q.; Frenkel, A. I.; Guo, W.; Hill, C.; Smith, C.; Kollar, J.; Troya, D.; Morris, J. R., Mechanism and Kinetics for Reaction of the Chemical Warfare Agent Simulant, DMMP(g), with Zirconium(IV) MOFs: An Ultrahigh-Vacuum and DFT Study. *J. Phys. Chem. C.* **2017,** *121* (21), 11261-11272.
5. Øien-Ødegaard, S.; Bouchevreau, B.; Hylland, K.; Wu, L. P.; Blom, R.; Grande, C.; Olsbye, U.; Tilset, M.; Lillerud, K. P., UiO-67-type Metal-Organic Frameworks with Enhanced Water Stability and Methane Adsorption Capacity. *Inorg. Chem.* **2016,** *55* (5), 1986-1991.